Photonic crystal fiber tip interferometer for refractive index sensing

Zhang, Taishi; Lim, Jun Long; Milenko, Karolina; Hu, Dora Juan Juan; Shum, Perry Ping; Wang, Yixin; Wolinski, Tomasz R.; Wei, Huifeng; Tong, Weijun

2012

Milenko, K., Hu, D. J. J., Shum, P. P., Zhang, T., Lim, J. L., Wang, Y., et al. (2012). Photonic crystal fiber tip interferometer for refractive index sensing. Optics Letters, 37(8), 1373-1375.

https://hdl.handle.net/10356/99327

https://doi.org/10.1364/OL.37.001373

Photonic crystal fiber tip interferometer for refractive index sensing

Karolina Mileńko,[1,2,3] Dora Juan Juan Hu,[3,*] Perry Ping Shum,[2] Taishi Zhang,[2,3] Jun Long Lim,[3] Yixin Wang,[3] Tomasz R. Woliński,[1] Huifeng Wei,[4] and Weijun Tong[4]

[1]*Faculty of Physics, Warsaw Univ. of Technology, Warsaw, Poland*

[2]*School of Electrical and Electronic Engineering, Nanyang Technological University, Singapore*

[3]*RF&Optical Department, Institute for Infocomm Research, Agency for Science, Technology and Research (A*STAR), Singapore*

[4]*State Key Laboratory of Optical Fiber and Cable Manufacture Technology, Yangtze Optical Fiber and Cable Company Ltd. Research & Development Center, China*

**Corresponding author: jjhu@i2r.a-star.edu.sg*

Received November 18, 2011; revised January 19, 2012; accepted February 3, 2012; posted February 6, 2012 (Doc. ID 158341); published April 12, 2012

In this paper we present an interferometer based on photonic crystal fiber (PCF) tip ended with a solid silica-sphere for refractive index sensing. The sensor is fabricated by splicing one end of the holey PCF to a single mode fiber (SMF) and applying arc at the other end to form a solid sphere. The sensor has been experimentally tested for refractive index and temperature sensing by monitoring its wavelength shift. Measurement results show that the sensor has the resolution of the order of 8.7×10^{-4} over the refractive index range of 1.33–1.40, and temperature sensitivity of the order of 10 pm/°C in the range of 20–100 °C.

OCIS codes: 060.2370, 060.5295, 120.3180.

Refractive index sensors show great promise in biological and chemical applications. Simple and compact refractometers can be used industrially, environmentally, clinically, and to monitor food processing. In recent years, optical fiber sensors for liquid refractive index sensing have gained more interest. They have many important advantages; they are light-weight, small, and have high sensitivity. They are immune to electromagnetic fields and have the potential for remote and real-time detection. Different structures of optical fiber sensors have been previously proposed, including surface plasmon resonance and etch fiber Bragg grating [1]. However, in those types of sensors the part of the cladding has to be removed to obtain overlap between the sample and optical field. We can overcome this drawback by using sensors based on photonic crystal fiber (PCF) interferometers. PCF-based interferometers have proved to have high sensitivity in a broad range of applications [2]. They are promising in the sensing of various physical parameters, such as temperature [3], strain [4], pressure [5], humidity [6], refractive index [7], and volatile organic compounds. In the optical fiber modal interferometer, light guided from the single mode fiber (SMF) diffracts when it reaches the collapsed region of the PCF. This diffraction causes mode broadening, which allows for the excitation of core and cladding modes in the PCF section. Excited higher order modes (HOMs) have relative phase difference compared with the fundamental mode, therefore the signal collected from the fiber end exhibits an interference pattern of the fundamental mode and HOMs. Higher order modes are sensitive to environmental parameters. Therefore, the interference pattern shift influenced by the refractive index of the surrounding medium can be utilized as the optical transduction mechanism. By monitoring the wavelength shift we can deduce changes in the external refractive index. Because the spectral pattern of the interferometer shows a periodic sinusoidal curve, the maximum sensing range is restricted by the curve's period, i.e., free spectral range (FSR).

In this paper we present a simple modal interferometer based on a holey PCF tip. We demonstrate the fabrication method by using an SMF spliced to a small section of the PCF. Experimental measurements are carried out by immersing the sensor in the liquid of the refractive index in the range of 1.331.40. By monitoring the wavelength shift we can deduce the external refractive index and its changes. Temperature sensitivity of the sensor is also investigated. The size of the sensor and reflection mode operation opens up a possibility for point sensing, and the volume of the tested sample is small.

The photonic crystal fiber used to create the sensor tip was fabricated in China by Yangtze Optical Fiber and Cable Company Ltd. (YOFC, China) by using a modified conventional optical fiber drawing process. Figure 1 shows a scanning electron microscope (SEM) picture of the utilized PCF. It is an index-guiding, air-silica PCF with a hexagonal lattice. The fiber cladding diameter is 125 μm, the pitch size $\Lambda 1 = 5.3$ μm (outer), $\Lambda 2 = 6.1$ μm (inner) and hole diameter $d1 = 2.8$ μm (outer), $d2 = 5.8$ μm (inner), and core diameter of 3.3 μm.

The sensor was fabricated by using only a conventional fiber cleaver and a fusion splicer. One end of the PCF was spliced to an SMF; splicing parameters were chosen to create a section of the PCF with fully collapsed air holes. The length of the collapsed region is 0.175 mm. Next, the other end of the PCF was placed between the

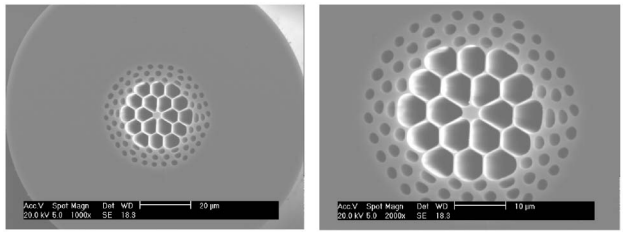

Fig. 1. Scanning electron microscope (SEM) picture of the employed PCF cross section.

0146-9592/12/081373-03$15.00/0

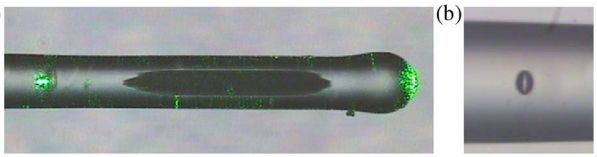

Fig. 2. (Color online) (a) Microscopic picture of the fabricated sensor head. (b) Close-up of an air bubble.

splicer electrodes and rearced, forming a solid sphere. The solid sphere at the end of the tip acts as a reflector [8]. The sensor created in this way has a compact size, and the length of the sensor head is 0.867 mm. The splice shows high strength, ensuring stable and long-term operation of the device (Fig. 2).

Under the splicing, an air bubble was formed in the SMF and PCF splice region. The working principle of the sensor is as follows: when the light propagating in an SMF reaches the splice region with the PCF, it diffracts because of the air bubble that works as a diverging lens, and the cladding modes are excited. Modes propagating through the PCF are reflected back when they reach the spherical surface at the end of the device. The device works as a Michelson interferometer (MI) with a multi-beam interference. The core and cladding modes having relative phase difference interfere when reaching the splicing point again. The excited cladding modes are highly sensitive to external changes in refractive index. Figure 2 shows a microscopic picture of the fabricated sensor and a close-up on the air bubble. The size of the air bubble is 17 μm. The green light source is launched in to the fiber, and two reflection mirrors are visible: at the air bubble and at the end of the fiber tip. The overall spectrum of the sensor as measured in alcohol and in glycerin, as shown in Fig. 3. We observed two interference patterns. The smaller FSR is influenced by the sensor lenght. The FSR can be calculated by using [9]:

$$\mathrm{FSR} = \lambda^2/2nz, \tag{1}$$

where λ is the wavelength of the propagated light, n is the refractive index of the fiber, and z is the length of the interferometer. Calculated FSR of the small fringes is 0.93 μm, whereas the measured is 0.86 μm. Wider modulation is caused by the air bubble in the splice region. By comparing the spectrum after dipping the sensor in alcohol and glycerin, we can see that interference caused by the air bubble is preservedthere is no wavelength shift or intensity change.

To confirm that wider modulation is caused by the air bubble, we calculated the interference of light reflected from the air bubble as a FabryPerrot cavity. The multiple

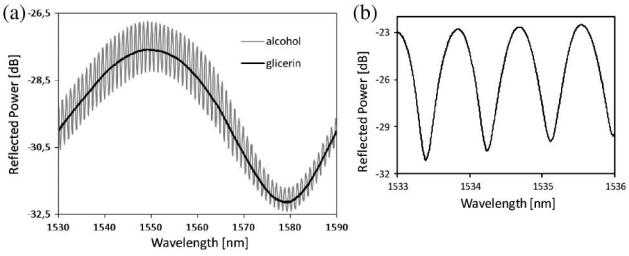

Fig. 3. (a) Overall spectrum of the sensor. (b) Sensor spectrum in chosen wavelength range.

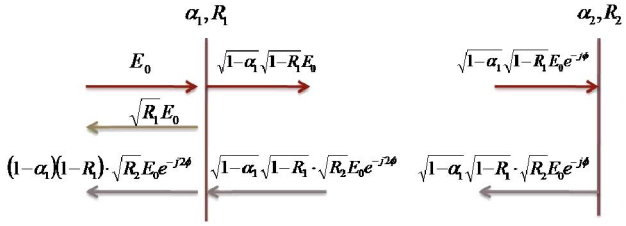

Fig. 4. (Color online) Multiple reflection model of the air bubble.

reflection model of the electric fields is derived with two-beam approximation and illustrated in Fig. 4. For simplification, the spherical shape of the cavity is not modeled. The total reflected electric fields are estimated by the sum of the total reflected electric fields from the two mirrors:

$$E_R = E_0\left[\sqrt{R_1} + (1-\alpha_1)^2(1-R_1)^2\sqrt{R_2}e^{-j2\phi_1}\right] \tag{2}$$

where, E_0 is the input electric field, and

$$R_i = \left(\frac{n_i - n_{i+1}}{n_i + n_{i+1}}\right)^2, \qquad i = 1,2 \tag{3}$$

are the reflection coefficients at the mirrors, where n_i represents the refractive indices in the SMF, air bubble, and the PCF respectively. α_i $(i = 1, 2)$ is the transmission loss at the i-th mirror, ϕ_i $(i = 1)$ is the phase shift cavity defined by:

$$\phi_i = \frac{2\pi n_i L_i}{\lambda} \qquad i = 1, \tag{4}$$

where L_i is the distance between two mirrors at air bubble size. The interference spectrum of the reflected light:

$$\begin{aligned} I_R &= \left|\frac{E_R}{E_0}\right|^2 \\ &= R_1 + (1-\alpha_1)^2(1-R_1)^2R_2 \\ &\quad + (1-\alpha_1)^2(1-\alpha_2)^2(1-R_1)^2(1-R_2)^2 \\ &\quad + 2(1-\alpha_1)(1-R_1)\sqrt{R_1R_2}\cos(2\phi_1). \end{aligned} \tag{5}$$

By comparing the calculated interference spectrum with the interference spectrum measured in glycerin, we can see that simulations and the experiment agree, with the slate change caused by disregarding the spherical shape of the air bubble (Fig. 5).

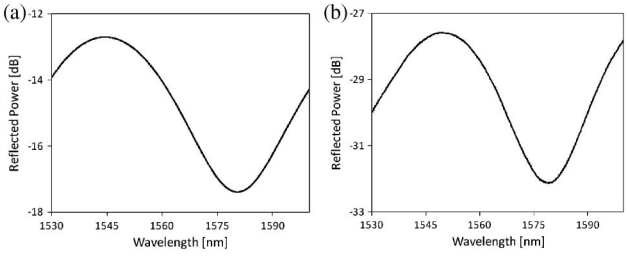

Fig. 5. (a) Calculated interference spectrum of the air bubble. (b) Measured spectrum in glycerin.

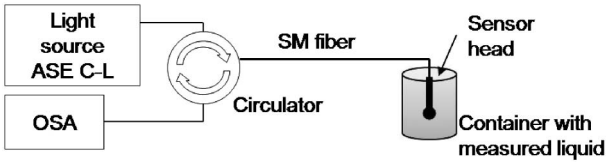

Fig. 6. Experimental setup consists of an ASE light source, optical spectrum analyzer (OSA), and three-port circulator.

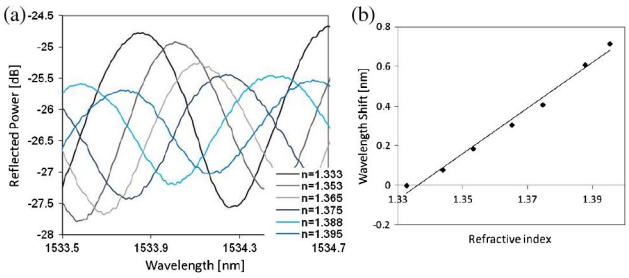

Fig. 7. (Color online) (a) Reflected power for different refractive indices in a wavelength function. (b) Deep position as a function of the refractive index of the surrounding medium.

The experimental setup is presented in Fig. 6. An ASE C-L band laser is used as a light source, and it is connected via a three-port circulator; the power of light reflected from the sensor head is detected by the optical spectrum analyzer (OSA). The spectrum collected by the OSA is distributed on a wide wavelength range (1530–1590 nm), and we observe stable interference pattern (Fig. 3(a)).

Refractive index measurements are carried out by immersing the sensor head in the liquid of some known refractive indices in the range of 1.33–1.40 RIU. Changes in the refractive index of the surrounding medium causes changes in the sensor spectrum. When the refractive index of the surrounding medium rises, we observe wavelength shift in to the higher wavelengths as well as an intensity change (Fig. 7(a)).

The wavelength shift is a linear function of the surrounding refractive index (Fig. 7(b)). Measurement results show that the sensor refractive index sensitivity is 11.5 nm/RIU and the resolution is of the order of 8.7×10^{-4} over the refractive index range of 1.331.40.

Changes in intensity can be used to calculate interference visibility according to the equation

$$V = \frac{I_{R\max} - I_{R\min}}{I_{R\max} + I_{R\min}}, \tag{6}$$

where $I_{R\max}$ and $I_{R\min}$ and are maximum and minimum light intensity.

Fringe visibility is a linear function of the surrounding refractive index; the total visibility change is 0.027 in the measured refractive index range (Fig. 8).

The influence of temperature is measured by placing a sensor in the oven and heating it from 25° to 100 °C. As a result of increasing temperature, we observe a wavelength shift into higher wavelengths (Fig. 9(a)). Changes in temperature do not influence light intensity collected by the OSA.

A deep position in the function of temperature is shown in Fig. 9(b), and the sensor shows a linear response to temperature changes. Calculated temperature sensitivity for the device is of the order of 10 pm/°C in the range of 25100 °C.

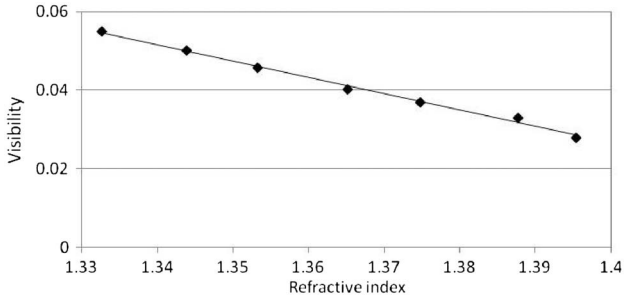

Fig. 8. Fringe visibility of the sensor.

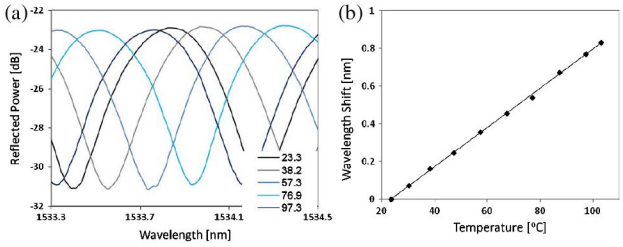

Fig. 9. (Color online) (a) Reflected power for different temperature in a wavelength function. (b) Deep position in the function of temperature.

We have demonstrated a photonic crystal fiber based modal interferometer ended with a solid silica sphere tip. We have shown that the refractive index of the surrounding medium causes a wavelength shift and intensity change in sensor response. Measurement results show that the sensor has a resolution of the order of 8.7×10^{-4} over the refractive index range of 1.331.40 and temperature sensitivity 10 pm/°C in the range of 25–100 °C. The influence of the air bubble in the splice region was also described. A great advantage of the presented sensor is its compact size, which allows us to measure small volumes of liquid samples.

This work was supported by the Infuse Exploratory Grant I02-0331-03 and by the Foundation for Polish Science in the frame of "Master Program."

References

1. N. Chryssis, S. M. Lee, S. B. Lee, S. S. Saini, and M. Dagenais, IEEE Photon. Technol. Lett. **17**, 1253 (2005).
2. J. Villatoro, V. Finazzi, G. Badenes, and V. Pruneri, J. Sens. **2009**, 747803 (2009).
3. J. Kou, J. Feng, L. Ye, F. Xu, and Y. Lu, Opt. Express **18**, 14245 (2010).
4. J. Villatoro, V. Finazzi, V. P. Minkovich, V. Pruneri, and G. Badenes, Appl. Phys. Lett. **91**, 091109 (2007).
5. W. J. Bock, T. A. Eftimov, P. Mikulic, and J. Chen, J. Lightwave Technol. **27**, 3933 (2009).
6. J. Mathew, Y. Semenova, G. Rajan, and G. Farrell, Electron. Lett. **46**, 1341 (2010).
7. R. Jha, J. Villatoro, G. Badenes, and V. Pruneri, Opt. Lett. **34**, 617 (2009).
8. N.-K. Chen, K.-Y. Lu, J.-T. Shy, and C. Lin, Opt. Lett. **36**, 2074 (2011).
9. W. C. Wong, C. C. Chan, L. H. Chen, Z. Q. Tou, and K. C. Leong, Opt. Lett. **36**, 1731 (2011).